Proceedings of the 21st ICSMGE, Vienna, Austria, 14 – 19 June 2026. Pistrol, Adam & Schweiger (eds.)
Published by: ÖGG, Austrian Society for Geomechanics, Salzburg, Austria, ISBN 978-3-9503898-4-5
https://doi.org/10.53243/ICSMGE2026-1587

Influence of precipitation kinetics on pore morphology during the biomineralization process

Daehyun Kim
Department of Civil and Environmental Engineering, The University of Suwon, Gyeonggi, Republic of Korea
dkim@suwon.ac.kr

Dimitrios Terzis, Lyesse Laloui
BIOGEOS, Swiss Federal Technology Institute of Lausanne (EPFL), Lausanne, Switzerland

Eugene Ee, Tae Sup Yun
School of Civil and Environmental Engineering, Yonsei University, Seoul, Republic of Korea

ABSTRACT: This research explores how the kinetics of biomineralization influence the evolution of pore structures in soils treated with biocementation. Biomineralization is recognized for its ability to improve soil strength and decrease permeability, supporting a range of geotechnical applications. During the treatment process, the infiltration of reactive solutions triggers precipitation reactions in real time, reshaping the internal pore network. Understanding the interplay between reaction rate, the scale of precipitation, and pore-scale alterations is essential for accurate and reliable engineering design. To investigate this, simulations were conducted in which the maximum size of precipitated minerals was systematically varied, and the associated changes in pore complexity were quantified through measurements of internal specific surface area and tortuosity. Three kinetic conditions—fast, moderate, and slow—were modeled to simulate precipitation within a porous matrix. Findings indicate that tortuosity consistently increases while porosity declines linearly as precipitation advances. The normalized internal specific surface area displayed distinct patterns for each reaction rate: a rise in fast reactions, stability under moderate rates, and a decline in slow reaction. These outcomes emphasize the significant role of reaction kinetics in defining pore morphology and provide valuable guidance for the design and implementation of biomineralization-based soil improvement techniques.

KEYWORDS: biocementation, biomineral formation; precipitation kinetics; pore morphology

1 INTRODUCTION

Biomineralization is a mineral-forming process driven by the metabolic activity of native microorganisms or naturally occurring enzymes, capable of producing stable compounds such as calcium carbonate ($CaCO_3$) within soil pore spaces. This in-situ mineral precipitation strengthens interparticle contacts, resulting in enhanced soil strength and reduced permeability (Cheng et al., 2013; DeJong et al., 2010; Kim et al., 2020; van Paassen et al., 2010). Although substantial progress has been made in elucidating the underlying mechanisms and evaluating the feasibility of field-scale applications, practical advancements in design optimization and large-scale deployment remain relatively scarce.

Many prior investigations have sought to link the volume of precipitated minerals to improvements in engineering behavior, yet the reported correlations often vary significantly. During treatment, reactive solutions traverse the intricate pore network, inducing precipitation that continually reshapes the soil's internal architecture. To achieve reliable geotechnical design and application, it is essential to clarify how reaction kinetics, precipitation rates, and spatial patterns of solution transport influence pore-scale structural transformations.

Emerging research indicates that, beyond the total mineral content, the resulting increase in pore morphological complexity plays a decisive role in modifying permeability, shear strength, and stiffness (Al Qabany & Soga, 2013; Martinez et al., 2013; Terzis and Laloui, 2018). Such complexity can be described through metrics including specific surface area, tortuosity, and pore connectivity—parameters that are closely tied to microscale transport dynamics, microbial colonization, and crystal growth behavior during the biomineralization process.

In this study, a numerical simulation approach was employed in which the maximum particle diameter of precipitated minerals was systematically adjusted to examine its impact on pore structural complexity. Quantitative evaluations were performed using specific surface area and tortuosity as the principal indicators of evolving pore geometry. The outcomes of this work aim to deepen understanding of the interplay between reaction conditions and pore-scale architecture, providing a scientific basis for the development of more precise and effective biomineralization-based soil improvement methodologies.

2 EXPERIMENTAL STUDY

2.1 *Preparation of biocemented soil sample*

X-ray Computed Tomography (XCT) imaging was employed to examine the internal microstructure of biocement-treated soil specimens composed of Itterbeck sand. The specimen was prepared under controlled laboratory conditions to ensure uniform treatment and minimize variability in material properties prior to imaging. XCT scanning was performed at a high spatial resolution, allowing precise visualization of the three-dimensional pore architecture and the distribution of mineral precipitates within the soil matrix. The raw cross-sectional slice was obtained from the scan (Figure 1a) was selected and was subsequently subjected to a comprehensive digital image processing workflow to accurately differentiate between soil grains, calcium carbonate ($CaCO_3$) deposits, and voids (Figure 1b).

The image analysis incorporated several sequential steps: (1) three-dimensional noise filtering to enhance image clarity, (2) threshold-based binary classification to separate solid and void phases, and (3) multiphase segmentation algorithms to distinguish individual components. Three processing steps were carefully calibrated to maintain phase boundary accuracy, thereby improving the reliability of quantitative measurements. Using the segmented datasets, the volumetric proportions and geometric attributes of each phase were quantitatively determined.

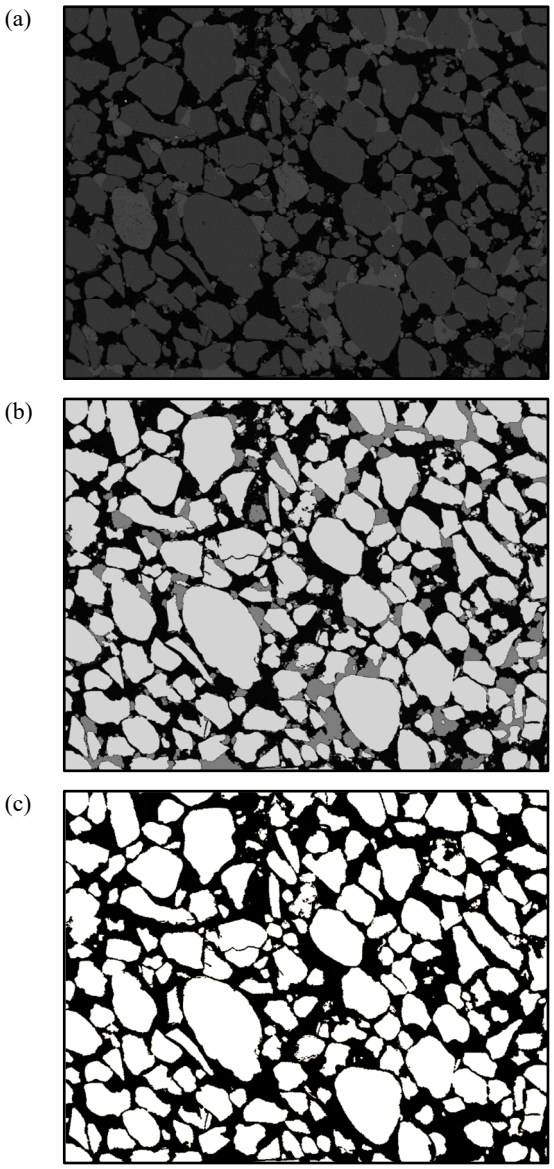

Figure 1. (a) Original XCT scan of the biocement-treated sample; (b) processed image following phase segmentation; (c) soil grain map generated after excluding precipitated minerals.

Quantitative results indicated that the total porosity decreased from 0.424 to 0.342 after biocementation, corresponding to an approximate reduction of 19.3%. This decrease can be attributed to extensive pore infilling and enhanced interparticle contact caused by $CaCO_3$ precipitation. The precipitate content was determined to be 14.55% of the oven-dried soil mass, reflecting a substantial degree of mineral accumulation within the pore network. These microstructural changes are significant because they directly influence macroscopic engineering properties. A reduction in porosity, coupled with particle bridging, is expected to lower hydraulic conductivity, increase stiffness, and improve shear resistance. Overall, these XCT-based observations confirm that biomineralization fundamentally modifies pore-scale architecture in ways that are directly relevant to geotechnical performance and durability.

2.2 *Numerical simulation of biomineral formation*

A numerical simulation of mineral precipitation was conducted using the previously generated soil grain map (Fig. 1c), applying a set of simplified modeling assumptions:

1. The biocementation solution is assumed to be evenly dispersed throughout the modeled domain.
2. Based on classical mineral nucleation theory, high reaction rates produce many small nuclei, while lower rates yield fewer but larger nuclei that subsequently grow.
3. Nucleation occurs randomly within pore spaces, avoiding pixels already occupied by soil grains, and each nucleus is idealized as a perfect circle.
4. Three kinetic conditions—fast, intermediate, and slow precipitation—are modeled using maximum precipitation diameters of 10, 50, and 100 μm, respectively.
5. Precipitates are permitted to overlap, allowing merged regions to exceed the specified maximum diameter or come into contact with soil grain surfaces.
6. The precipitation process proceeds until the accumulated mineral volume surpasses 30% of the oven-dried soil mass, at which point the simulation ends.

Every stage of mineral growth was captured as an image, which was then used to sequentially compute and record both porosity and mineral content. Figure 2 displays the final stage for each reaction scenario once the simulation reached completion.

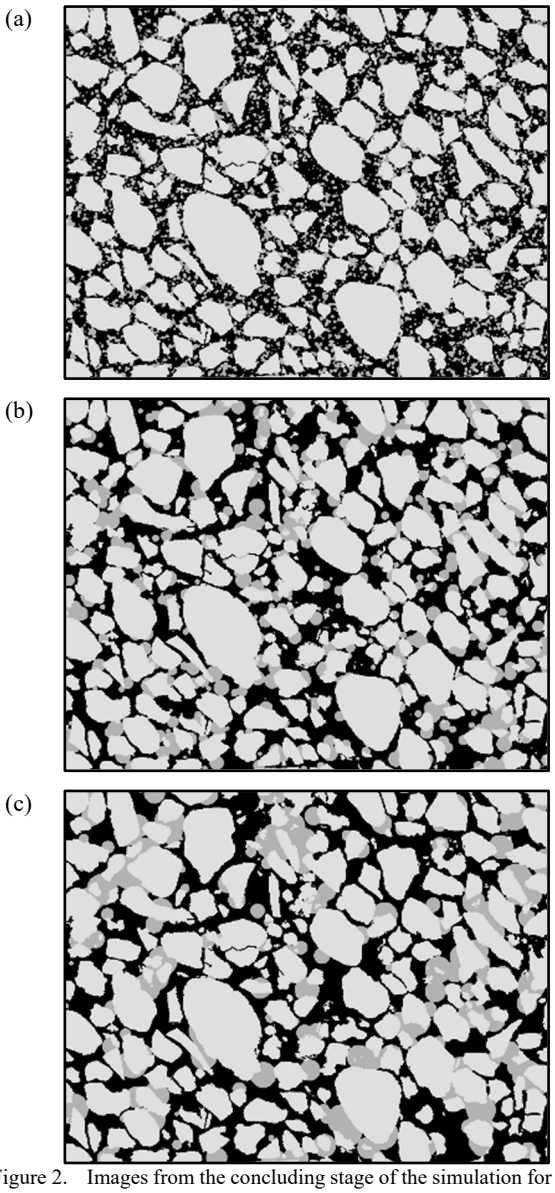

Figure 2. Images from the concluding stage of the simulation for each precipitation scenario: (a) fast reaction, maximum mineral size 10 μm; (b) moderate reaction, maximum mineral size 50 μm; (c) slow reaction, maximum mineral size 100 μm.

2.3 *Measurement of pore morphological parameters*

For every recorded stage of the simulation, the specific surface area was calculated from the processed pore-scale images, ensuring that a consistent methodology was applied across all precipitation scenarios. This approach allowed detailed monitoring of how surface characteristics evolved as mineral precipitation advanced, capturing even minor modifications in pore geometry over time. Once the specific surface area was determined, steady-state diffusion analyses were carried out on the same image datasets to evaluate transport behavior within the progressively altered pore network. These diffusion simulations modeled the movement of a tracer through interconnected void spaces, enabling the determination of the effective diffusion coefficient under each reaction condition.

Tortuosity, representing the degree of flow path complexity and elongation, was then derived using the Bruggeman relationship (1935), which establishes a correlation between the effective diffusion coefficient and the corresponding porosity obtained from the segmented images. This combined workflow established a direct connection between microstructural changes and transport properties, providing valuable insight into how biomineralization-induced alterations in pore structure influence diffusion resistance at the microscale.

3 RESULTS

3.1 *Alteration of pore morphological parameters - tortuosity*

Figure 3 presents the evolution of tortuosity across successive stages of the simulation, as derived from steady-state diffusion analyses performed on the series of pore-scale images. In this plot, each circular marker represents a tortuosity value calculated from an individual simulation snapshot, providing a step-by-step depiction of how the complexity of flow pathways changes as mineral precipitation progresses. The dashed lines in the figure indicate fitted trend curves, which are intended to clarify the general direction and magnitude of change over time rather than to serve as predictive models.

Among the three modeled reaction scenarios, the fast-precipitation condition—with a maximum mineral particle diameter of 10 µm—demonstrated the steepest and most consistent increase in tortuosity throughout the simulation. This pronounced rise can be attributed to the widespread formation of numerous small mineral clusters that intersect and partially obstruct existing flow channels, forcing diffusive transport along increasingly convoluted paths. Such structural changes significantly enhance the effective path length for transport processes, thereby increasing resistance to fluid or solute movement.

The intermediate-precipitation case, defined by a maximum particle diameter of 50 µm, displayed a more moderate yet steady upward trend in tortuosity. This suggests a balance between pore constriction due to precipitation and the preservation of partial flow pathways that remain relatively navigable. In contrast, the slow-precipitation scenario (maximum particle diameter of 100 µm) exhibited only a slight overall increase in tortuosity. Here, the fewer but larger precipitates tend to block specific sections of the pore network without extensively fragmenting the connectivity, thus maintaining relatively direct transport routes.

It should be noted that while trend lines were fitted to illustrate progression patterns, the explicit mathematical expressions are not included in this report due to their limited physical interpretability and the descriptive nature of this analysis.

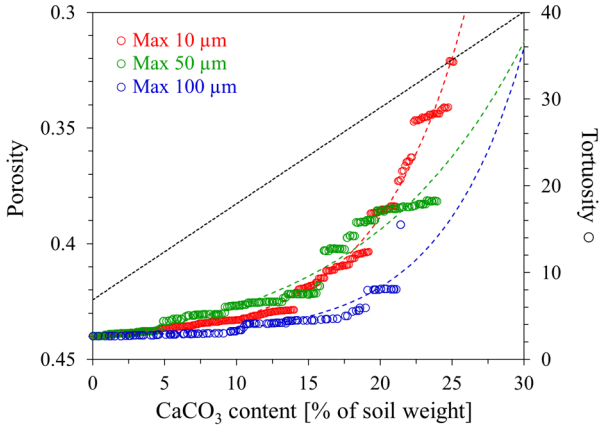

Figure 3. Variation of tortuosity derived from steady-state diffusion analyses.

3.2 *Alteration of pore morphological parameters – internal specific surface area*

Figure 3 presents the variation in normalized specific surface area, calculated as the ratio of the instantaneous value to that of the untreated specimen, plotted against the extent of mineral precipitation. This normalization allows direct comparison between the different reaction scenarios by eliminating the influence of the initial microstructural differences and focusing on relative changes over time.

In contrast to the tortuosity trends described in Section 3.1, the evolution of specific surface area exhibited clear divergences among the three precipitation rates. The fast-precipitation scenario, characterized by a maximum particle diameter of 10 µm, demonstrated a persistent and steady increase in specific surface area as precipitation progressed. This pattern reflects the proliferation of fine mineral deposits that coat and bridge pore surfaces, generating a higher degree of textural complexity. The widespread nucleation of small particles not only constricts flow pathways but also creates additional surface irregularities, thereby enhancing the total interfacial area available within the pore network.

The intermediate-rate case, with a maximum particle diameter of 50 µm, maintained a nearly constant specific surface area throughout the simulation. This stability suggests that the rates of pore blockage and new surface generation were approximately balanced. Precipitation events in this scenario tended to partially occlude pore throats without significantly altering the remaining pore walls, leading to a dynamic equilibrium between surface loss and surface creation.

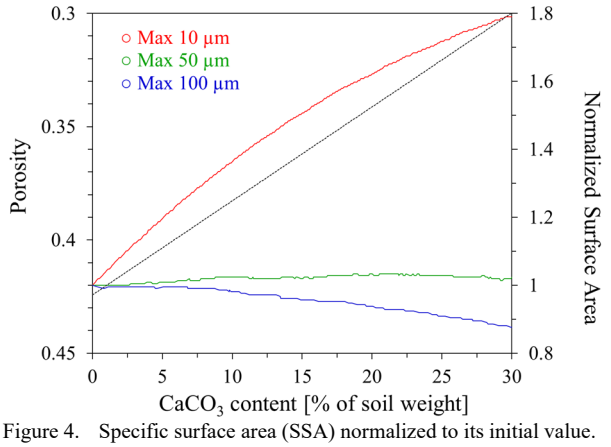

Figure 4. Specific surface area (SSA) normalized to its initial value.

In the slow-precipitation scenario, defined by a maximum particle diameter of 100 μm, the normalized specific surface area gradually declined. This reduction is attributed to the preferential growth of fewer, larger crystals, which tend to smooth or obscure existing pore surfaces and thus reduce the total measurable surface area.

These distinct behaviors reinforce the conclusion that precipitation kinetics strongly dictate microstructural evolution. For biomineralization-based soil improvement, this finding underscores the necessity of optimizing reaction rates to tailor pore-scale properties for targeted hydraulic, mechanical, or durability performance objectives.

4 CONCLUSIONS

This study employed XCT-based microstructural characterization and image-driven numerical simulations to investigate the influence of biomineralization kinetics on pore-scale morphological evolution in biocement-treated soils. The primary findings can be summarized as follows:

1. Porosity reduction and mineral accumulation – XCT analysis revealed that biocementation treatment reduced total porosity by approximately 19.3%, accompanied by substantial calcium carbonate precipitation equivalent to 14.55% of the oven-dried soil mass. These changes reflect significant pore infilling and enhanced interparticle bonding.
2. Tortuosity evolution – Numerical simulation results demonstrated that reaction rate strongly governs tortuosity growth. The fast-precipitation scenario produced the steepest increase due to the formation of numerous fine mineral clusters, whereas the slow-precipitation scenario resulted in minimal changes, maintaining relatively direct flow paths.
3. Specific surface area trends – Normalized specific surface area displayed distinct kinetic-dependent patterns: continuous growth in the fast-precipitation case, near-stability in the intermediate case, and gradual decline in the slow case. These trends indicate a balance (or imbalance) between surface generation and loss, depending on precipitation behavior.
4. Engineering implications – The combined analysis of tortuosity and specific surface area highlights that reaction kinetics affect not only the quantity but also the spatial configuration of mineral deposits, with direct consequences for permeability, mechanical stiffness, and shear strength.

Overall, these results underscore the necessity of incorporating kinetic control into the design of biomineralization-based ground improvement strategies. Optimizing parameters such as solution chemistry, injection protocol, and microbial activity should consider both the amount and distribution of precipitates to achieve targeted pore-scale properties. Future research should validate these simulation-based findings through time-resolved in-situ imaging and explore coupled mechanical–hydraulic modeling to link microstructural changes directly to macroscopic performance.

5 ACKNOWLEDGEMENTS

This research was supported by Basic Science Research Program through the National Research Foundation of Korea (NRF) funded by the Ministry of Education (No. RS-2023-00250736).

6 REFERENCES

Bruggeman, V. D. (1935). Berechnung verschiedener physikalischer Konstanten von heterogenen Substanzen. I. Dielektrizitätskonstanten und Leitfähigkeiten der Mischkörper aus isotropen Substanzen. Annalen der physik, 416(7), 636-664.

Cheng, L., Cord-Ruwisch, R., and Shahin, M. A. (2013). Cementation of sand soil by microbially induced calcite precipitation at various degrees of saturation. Canadian Geotechnical Journal, 50(1), 81-90.

DeJong, J. T., Mortensen, B. M., Martinez, B. C., and Nelson, D. C. (2010). Bio-mediated soil improvement. *Ecological engineering*, 36(2), 197-210.

Kim, D., Mahabadi, N., Jang, J., and van Paassen, L. A. (2020). Assessing the kinetics and pore-scale characteristics of biological calcium carbonate precipitation in porous media using a microfluidic chip experiment. *Water Resources Research*, 56(2), e2019WR025420.

Martinez, B. C., DeJong, J. T., Ginn, T. R., Montoya, B. M., Barkouki, T. H., Hunt, C., ... and Major, D. (2013). Experimental optimization of microbial-induced carbonate precipitation for soil improvement. *Journal of Geotechnical and Geoenvironmental Engineering*, 139(4), 587-598.

Qabany, A. A., and Soga, K. (2014). Effect of chemical treatment used in MICP on engineering properties of cemented soils. *In Bio-and chemo-mechanical processes in geotechnical engineering: géotechnique symposium in print 2013* (pp. 107-115). ICE Publishing.

Terzis, D., and Laloui, L. (2018). 3-D micro-architecture and mechanical response of soil cemented via microbial-induced calcite precipitation. *Scientific reports*, *8*(1), 1416.

Van Paassen, L. (2009), Biogrout: Ground improvement by microbially induced carbonate precipitation, Delft University of Technology.